






Magnetization switching by spin-orbit torque in crystalline (Ga,Mn)(As,P) film deposited on a vicinal GaAs substrate

Apu Kumar Jana ¹, Kyung Jae Lee ¹, Sanghoon Lee ^{1,*}, Xinyu Liu ², Margaret Dobrowolska,² and Jacek K. Furdyna ²

¹*Physics Department, Korea University, Seoul 136-701, Republic of Korea*

²*Department of Physics and Astronomy, University of Notre Dame, Notre Dame, Indiana 46556, USA*



(Received 12 March 2024; revised 15 June 2024; accepted 22 July 2024; published 12 August 2024)

Current-induced spin-orbit torque (SOT) switching of magnetization in a crystalline (Ga,Mn)(As,P) ferromagnetic semiconductor (FMS) film grown on a vicinal GaAs substrate is investigated. The FMS film has four magnetic easy axes along the $\langle 100 \rangle$ directions in the (001) crystal plane. However, unlike FMSs such as (Ga,Mn)(As,P) grown on the (001) surface, in vicinal configuration, both in-plane and out of plane components of magnetization contribute to Hall resistance (HR). Thus the values of the HR are different when the magnetization is aligned along the different easy axes owing to the inclination of the film plane away from the (001) crystal plane. Current-induced magnetization transitions between easy axes are clearly observed in HR measurements in the absence of an external magnetic field, resulting in HR hysteresis loops as the current is scanned. Each hysteresis loop, however, reveals different stable states. The HR values corresponding to these states indicate that magnetization transitions between the adjacent easy directions are partial, the stable states being composed of sets of multiple domains magnetized along different easy directions. The stable states observed during the SOT magnetization switching are highly reproducible over a large number of current scans. The field-free multivalued SOT magnetization switching observed in such vicinal (Ga,Mn)(As,P) FMSs suggests the possibility of using vicinal FMS films for current-controlled, energy-efficient magnetic multinary memory devices.

DOI: [10.1103/PhysRevB.110.054422](https://doi.org/10.1103/PhysRevB.110.054422)

I. INTRODUCTION

Spin-orbit torque (SOT) has emerged as an important subject in the field of spintronics because of its potential for manipulating magnetization through application of electric current [1–3]. This capability has already found its way into various spintronic devices, such as SOT memory and logic gates, offering promising prospects for technological development [4–6]. In particular, SOT-based magnetic random access memories (MRAMs) are projected to outperform spin transfer torque (STT) MRAMs in terms of writing speed, energy efficiency, and endurance [1–6]. So far SOT investigations have been focused primarily on ferromagnetic-metal/heavy-metal (FM/HM) bilayer systems, where a spin current generated within the heavy-metal layer and at the interface between the two layers exerts a torque on the magnetization of the adjacent ferromagnetic layer, facilitating SOT magnetization switching [7,8].

Recently, attention in this area has been directed toward crystalline GaAs-based ferromagnetic semiconductors (FMSs), such as (Ga,Mn)(As) and (Ga,Mn)(As,P). These materials achieve spin polarization of current carriers through Dresselhaus and/or Rashba spin-orbit interactions originating from the inversion asymmetry within the crystal structure [9,10]. Remarkably, these FMS materials required current densities for SOT-induced magnetization switching that are one to two orders of magnitude lower than the FM/HM

systems [11,12]. Moreover, crystalline FMS films exhibit important magnetic anisotropy properties, including robust cubic and uniaxial anisotropy within the film plane, that can be directly exploited in SOT switching devices [13,14]. As an example, crystalline FMS films possessing two noncollinear in-plane easy axes exhibit a giant planar Hall effect (PHE) [15], which has the potential for magnetic memory applications. The presence of such two noncollinear (nearly orthogonal) in-plane easy axes also provides the opportunity of forming multidomain magnetic structures, suggesting prospects for multistate device applications [16,17] as well as for neuromorphic computation [18].

The opportunities for such multilevel magnetic state devices has already been noted in several instances involving various metallic ferromagnets [19–21] and crystalline FMS films [22–24] grown on vicinal surfaces. Briefly, the inclination of the (001) crystal plane relative to the film plane results in complex Hall resistance (HR) behavior involving both planar Hall resistance (PHR) and anomalous Hall resistance (AHR), which correspond, respectively, to contributions of in-plane and out of plane components of magnetization [23–25]. Such simultaneous PHR and AHR occurring in vicinal films then results in distinct HR values that are different when the magnetization is oriented along different easy axes, thus providing the opportunity for designing multistate memory functions [24]. However, manipulation of magnetization in the works referred to above relies on applying external magnetic fields, which is often impractical in device applications. Fortunately, significant strides have already been made in controlling magnetization by field-free SOT magnetization

*Contact author: slee3@korea.ac.kr

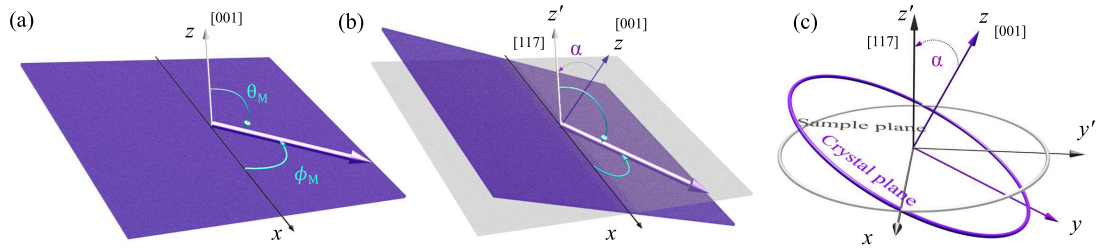


FIG. 1. (a) Schematic representation of film plane coincident with the (001) crystal plane in which magnetization resides (thick arrow). (b) Schematics of the (117) film plane (gray) and the (001) crystal plane (violet), with a tilt angle α between them. (c) Two coordinate systems, $S(x, y, z)$ and $S'(x', y', z')$, representing the crystal and the film planes, respectively.

switching in crystalline FMS films, facilitated by current pulses in the absence of external fields [26].

In the present study we investigate SOT switching in a single layer of crystalline (Ga,Mn)(As,P) ferromagnetic semiconductor film grown on a vicinal GaAs surface, exhibiting robust fourfold in-plane magnetic anisotropy. This unique configuration enables field-free SOT switching due to the spin polarization of current carriers induced by the spin-orbit field components aligned with the easy axes in the (001) crystal plane [26]. Importantly, it will be shown that, owing to the inclination of the (001) crystal plane relative to the film plane, changes in magnetization orientation between different easy axes result in multiple values of HR, which can be exploited for designing multistate memory devices and memristors for a variety of applications, including neuromorphic computing [18,27].

II. HALL RESISTANCE IN CRYSTALLINE FMS FILMS GROWN ON A VICINAL SURFACE

Hall resistance (HR) of a ferromagnetic film in the presence of an applied magnetic field is given by

$$\text{HR} = \frac{R_o}{t} H_{\perp} + \frac{R_s}{t} M_{\perp} + \frac{k}{t} M_{\parallel}^2 \sin 2\varphi_M, \quad (1)$$

where the first, second, and third terms are the normal Hall resistance, anomalous Hall resistance (AHR), and planar Hall resistance (PHR), respectively; H_{\perp} is the component of applied magnetic field \mathbf{H} normal to the film; M_{\perp} and M_{\parallel} are components of magnetization \mathbf{M} normal and parallel to the film plane; R_o and R_s are the normal and anomalous Hall coefficients, respectively; k is a constant related to the anisotropic magnetoresistance; φ_M is the azimuthal angle of in-plane magnetization. M_{\parallel} is measured from the current direction, and t is the thickness of the thin film. Since in ferromagnetic materials the normal Hall resistance is typically negligible compared to the other two terms, in what follows we will only consider the magnetization-dependent terms, so that [28,29]

$$\text{HR} = \frac{R_s}{t} M_{\perp} + \frac{k}{t} M_{\parallel}^2 \sin 2\varphi_M. \quad (2)$$

Let us first consider a (Ga,Mn)(As,P) film whose plane coincides with the (001) crystal plane [Fig. 1(a)]. In the case of films with strong cubic magnetic anisotropy of the material, when the magnetization \mathbf{M} is initialized in the film plane, it will remain in that plane, and magnetization transitions will occur between easy axes within that plane. Since in this

system $M_{\perp} = 0$, there will be no contribution from AHR, so that the value of HR is determined only by PHR. However, when the film plane (in which the current flows) is tilted (vicinal) relative to the (001) crystal plane, the M_{\perp} component in the sample coordinates is no longer zero, resulting in a finite AHR contribution to HR. The value of HR will then consist of contributions from AHR and PHR, as shown in Eq. (2).

An example of this case is a crystalline (Ga,Mn)(As,P) FMS film with strong in-plane anisotropy grown on a GaAs vicinal surface [22–24], as shown in Fig. 1(b). The film plane for HR measurement (drawn in gray) is tilted by an angle α relative to the crystal plane (violet) that contains the easy axes between which magnetization transitions occur.

To discuss HR in a crystalline FM film grown on a vicinal surface at a tilt angle α between the film and the crystal (001) plane (which contains the easy axes of magnetization \mathbf{M}), one needs to express the components of \mathbf{M} in film coordinates. To obtain the relationship between measured HR and the vicinal angle α , we use two coordinate systems, $S(x, y, z)$ and $S'(x', y', z')$, representing the crystal coordinates (violet) and the film coordinates (gray), respectively, as shown in Fig. 1(c). These two coordinates are related through the rotation matrix given by [30,31]

$$R_x(\alpha) = \begin{pmatrix} 1 & 0 & 0 \\ 0 & \cos \alpha & \sin \alpha \\ 0 & -\sin \alpha & \cos \alpha \end{pmatrix}. \quad (3)$$

Under such transformation, the magnetization \mathbf{M}' measured in the film plane [i.e., in the $S'(x', y', z')$ frame] can be expressed as

$$\begin{aligned} \begin{pmatrix} M'_x \\ M'_y \\ M'_z \end{pmatrix} &= \begin{pmatrix} 1 & 0 & 0 \\ 0 & \cos \alpha & \sin \alpha \\ 0 & -\sin \alpha & \cos \alpha \end{pmatrix} \begin{pmatrix} M_x \\ M_y \\ M_z \end{pmatrix} \\ &= \begin{pmatrix} M \cos \varphi_M \\ M \sin \varphi_M \cos \alpha \\ -M \sin \varphi_M \sin \alpha \end{pmatrix}. \end{aligned} \quad (4)$$

Note that due to the tilt α we now have in the film coordinate system a perpendicular component of magnetization, $M'_z = -M \sin \varphi_M \sin \alpha$, and the component of \mathbf{M}' measured in the film plane is

$$\begin{aligned} M'_{\parallel} &= (M'^2_x + M'^2_y)^{1/2} = M(\cos^2 \varphi_M + \sin^2 \varphi_M \cos^2 \alpha)^{1/2} \\ &= M(1 - \sin^2 \varphi_M \sin^2 \alpha)^{1/2}. \end{aligned}$$

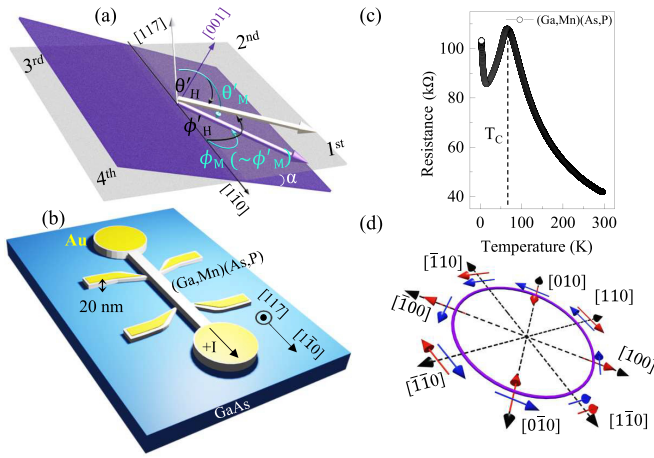


FIG. 2. (a) Schematic representation of the film plane (gray) and the (001) crystal plane (violet), tilted with respect to each other by angle α of $\sim 11.42^\circ$ in the $(1\bar{1}0)$ plane. The polar angle of magnetization (θ'_M) is measured from the [117] direction, and the azimuthal angle (φ'_M) is measured counterclockwise (CCW) from the [110] direction, which is the positive current direction. Quadrants 1–4 are indicated in the film (gray) plane. (b) Schematic of the Hall bar. (c) Temperature dependence of resistance, showing Curie temperature (T_C) of about 65 K. (d) Directions of Dresselhaus (red arrows) and Rashba (blue arrows) SOFs in the (Ga,Mn)(As,P) film shown for various current directions (black dashed arrows).

The Hall resistance in Eq. (1) for the FM film grown on a vicinal surface can then be written as

$$\text{HR} = -\frac{R_s}{t} M \sin \varphi_M \sin \alpha + \frac{k}{t} M^2 (1 - \sin^2 \varphi_M \sin^2 \alpha) \sin 2\varphi'_M. \quad (5)$$

Note that in Eq. (5) φ_M is in crystal coordinates and φ'_M is in film coordinates. However, the difference between φ'_M and φ_M is negligible with small α , and we can rewrite Eq. (5) as

$$\text{HR} = -\frac{R_s}{t} M \sin \varphi'_M \sin \alpha + \frac{k}{t} M^2 (1 - \sin^2 \varphi'_M \sin^2 \alpha) \sin 2\varphi'_M, \quad (6)$$

which we will use to analyze the HR values when we investigate SOT switching in our vicinal (Ga,Mn)(As,P) film.

III. EXPERIMENTAL PROCEDURE

A (Ga,Mn)(As,P) film (Mn $\sim 7\%$ and P $\sim 9\%$) of thickness 20 nm was grown on a vicinal (117) GaAs substrate by using molecular beam epitaxy (MBE) in a 32 R&D MBE machine equipped with elemental sources of Ga, Mn, As, and P. The orientations of magnetization (violet thick arrow) and magnetic field (white thick arrow) during measurements are shown in Fig. 2(a). The angle α of approximately $\sim 11.42^\circ$ indicates the inclination between the (001) crystal plane and the (117) film plane. The inclination of the vicinal surface is along the [110] crystal direction. Since the structural properties of (Ga,Mn)(As,P) films grown by the same MBE technique have

been extensively studied in previous works [32,33], we focused solely on the SOT experiment in this investigation.

For transport measurements, a Hall bar was patterned by photolithography and dry etching. As shown in Fig. 2(b), the Hall bar is rectangular, 2.0 mm long by 20 μm wide. The current channel is aligned with the [110] direction. The sign of the current is defined as positive when the current is directed along [110], and negative when it is along $[\bar{1}10]$. The Curie temperature T_C of the (Ga,Mn)(As,P) film is estimated as 65 K from the temperature dependence of the resistance shown in Fig. 2(c) [34].

In the experiment, the azimuthal angles of magnetization φ'_M and of external field φ_H are measured counterclockwise (CCW) from the [110] direction in the film plane, as shown in Fig. 2(a). Note that in our case the direction [110] is the same in crystal and in film coordinate systems. We number the four quadrants in the crystal plane, proceeding CCW from the [110] direction, as shown in Fig. 2(a). For investigating magnetic anisotropy, angular scans of HR were carried out as the magnetic field of constant magnitude was rotated in the film plane, with a current of 10 μA (current density of $J = 2.5 \times 10^3 \text{ A/cm}^2$), which is sufficiently weak to have negligible Joule heating and spin-orbit torque (SOT) effects. Current-induced spin-orbit fields (SOFs) arising from Dresselhaus and Rashba effects, which spin polarize the current, become important at higher current values. Directions of the Dresselhaus and Rashba SOFs are indicated in Fig. 2(d) by red and blue arrows, respectively, the current directions being shown by black dashed arrows. In the present case both Rashba and Dresselhaus point in the same direction [110], 90° measured counterclockwise from the current flow.

IV. MAGNETIC ANISOTROPY AND HALL RESISTANCE

In studies of magnetization switching by SOT in a (Ga,Mn)(As,P) film grown on a vicinal surface, information on magnetic anisotropy and on the contributions of planar Hall resistance (PHR) and anomalous Hall resistance (AHR) to the measured Hall resistance (HR) are of key importance for identifying the states of magnetization. To obtain this information, we first performed HR measurements by rotating a constant external magnetic field in the film plane. Figure 3(a) shows representative HR data obtained as a function of the azimuthal angle in the film plane using an applied field of 300 Oe at 3 K. (Data obtained with other field strengths are shown in Supplemental Fig. 1 in the Supplemental Material [35]). The data clearly show four stable states as the field is rotated over 360° , indicating fourfold in-plane magnetic anisotropy. Importantly, even though magnetization transitions occur regularly every 90° , the values of HR at the stable states (i.e., marked as A–D between transitions in the figure), are different. This is because the combined contributions of the in-plane and out of plane components of magnetization aligned with different $\langle 100 \rangle$ easy axes to HR measured in the (117) vicinal plane are different at each magnetization transition [22–24].

To identify the AHR and PHR contributions to HR, we deconvoluted the angular scan HR data shown in Fig. 3(a) into $\sin 2\varphi'_M$ and $\sin \varphi'_M$ components, which, as seen in Eq. (6), correspond to contributions from the in-plane and the out of plane components of magnetization M' to HR, as shown by

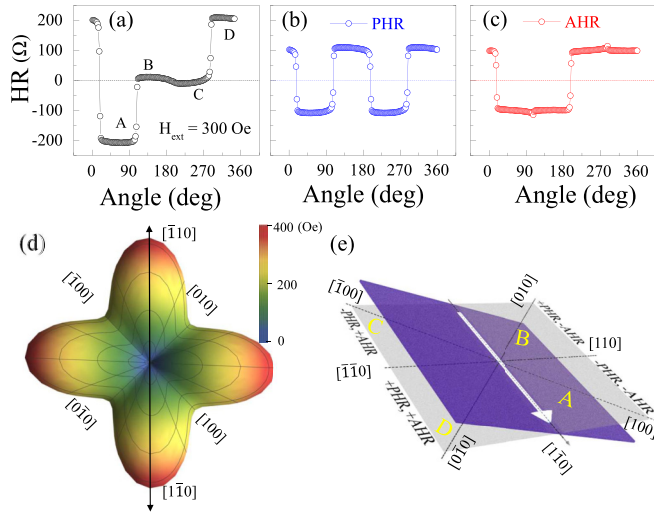


FIG. 3. (a) HR data obtained by rotating a 300 Oe magnetic field in the film plane at 3 K. Stable HR states marked as A–D correspond to HR values in the first through fourth quadrants, respectively. (b) PHR (blue open symbols) and (c) AHR (red open symbols) extracted from the HR data in (a), as discussed in the text. Note that AHR is negative in the entire 0° – 180° region (i.e., in the first and second quadrants) and positive in the 180° – 360° region (i.e., in the third and fourth quadrants). (d) Magnetic energy diagram for the sample, showing fourfold in-plane magnetic anisotropy. (e) Sign combinations of PHR and AHR for magnetization oriented along the four $\langle 100 \rangle$ easy axes, corresponding to states A–D shown in (a).

blue and red symbols in Figs. 3(b) and 3(c), respectively. (See also Supplemental Sec. 1 [35] for measurements at other field strengths.)

It is now well established that the in-plane anisotropy of the crystalline FMS film can be obtained by analyzing the angular dependence of PHR (i.e., data showing the $\sin 2\phi'_M$ behavior) based on free energy minima conditions [28,29]. The magnetic energy diagram obtained from our data (see Supplemental Sec. 1 [35]) is plotted in Fig. 3(d), which clearly shows a fourfold symmetry in the (001) crystal plane, with energy minima at the $\langle 100 \rangle$ directions and maxima at the $\langle 110 \rangle$ directions. The switching of magnetization will then occur between adjacent $\langle 100 \rangle$ crystal directions. In the vicinal coordinate system such switching will involve both in-plane and out of plane components of magnetization simultaneously, which will be reflected in the measured HR.

As seen in Figs. 3(b) and 3(c), the contributions of AHR caused by the out of plane component of magnetization have the sign sequence $-$, $-$, $+$, $+$ as M' progresses through the first, second, third, and fourth quadrants, respectively; while the contribution of PHR has the sign of sequence $-$, $+$, $-$, $+$ due to negative k for (Ga,Mn)(As,P) material [36], as shown in Fig. 3(e). Thus HR shows strong minima when magnetization is in the first quadrant ($-$ PHR, $-$ AHR) and strong maxima when it is in the fourth quadrant ($+$ PHR, $+$ AHR), as seen in Fig. 3(a). When the magnetization is in the second and third quadrants, however, the PHR and AHR contributions have opposite signs, compensating each other. This results in small HR values for the magnetization in these quadrants, as shown by states B and C in Fig. 3(a). As discussed above, cubic

anisotropy is dominant at 3 K in our (Ga,Mn)(As,P) film, but it is known that the magnetic anisotropy of GaAs-based FMS films varies sensitively with temperature [37]. To investigate SOT switching phenomena in the FMS film with well-defined magnetic easy axes along the $\langle 100 \rangle$ directions, we performed our SOT experiment at low temperatures.

V. SPIN-ORBIT TORQUE (SOT) SWITCHING OF MAGNETIZATION

The inversion asymmetry of zinc-blende crystals such as our (Ga,Mn)(As,P) produces an internal electric field. It is well known that when a current flows through a crystal with this structure, the electric field—when transformed relativistically to the frame of reference of a moving current carrier—gives rise to a magnetic field in the carrier frame, which then acts on the carrier spin through spin-orbit interaction, resulting in spin polarization of the current [38,39]. When such spin-polarized current flows through a ferromagnet, as in the case of our (Ga,Mn)(As,P) film, its spin will interact with the magnetization of the material by exerting a torque, referred to as spin-orbit torque (SOT). This in turn provides a means for manipulating the magnetization of the material (e.g., switching its direction from one easy axis to another) by an electric current. Importantly, such manipulation can be carried out in the absence of an external magnetic field.

In this paper such SOT switching of magnetization by an electric current in the absence of an external field is studied as follows. The magnetization of the (Ga,Mn)(As,P) film is initially set along one of the easy axes (e.g., $[100]$) by a field of 2000 Oe, which is removed before starting the current scan. Current scans of HR obtained at 3 K for magnetizations initialized along the four easy directions are shown in Fig. 4. The scan starts with the current in the positive direction (i.e., $[1\bar{1}0]$) when magnetization is initialized along $[100]$ and $[010]$, and in the negative (i.e., $[\bar{1}10]$) direction for magnetization initialized along $[\bar{1}00]$ and $[0\bar{1}0]$, so as to preserve symmetry. The star symbols in Figs. 4(a)–4(d) show the values of HR at initial magnetization of each scan, as shown in the insets.

Note that the initial HR values for the $[010]$ [Fig. 4(b)] and $[\bar{1}00]$ [Fig. 4(c)] initialization case are small negative ($\sim -5 \Omega$) and small positive ($\sim +5 \Omega$), respectively, while the B and C states shown in Fig. 3(a), corresponding to the $[010]$ and $[\bar{1}00]$ directions in the angle scan measurement, show small positive and negative HR values (i.e., opposite sign of HR). This inconsistency arises due to the presence of an external field in the angle scan measurement. For the initial points in the current scan measurement, the magnetic field (~ 2000 Oe) used for initialization is removed before the current scan starts as we discussed earlier. Magnetization at the $[010]$ (i.e., second quadrant) and $[\bar{1}00]$ (i.e., third quadrant) directions give $HR = +|\text{PHR}| - |\text{AHR}|$ and $HR = -|\text{PHR}| + |\text{AHR}|$, respectively, according to Eq. (6). In the absence of an external field, relative strength is $|\text{AHR}| > |\text{PHR}|$ and, thus, HR are small negative and small positive, respectively, at the $[010]$ and $[\bar{1}00]$ initialized directions in the current scan shown in Figs. 4(b) and 4(c). Contrarily, in the angle scan measurements [Fig. 3(a)], the 300 Oe field drags the

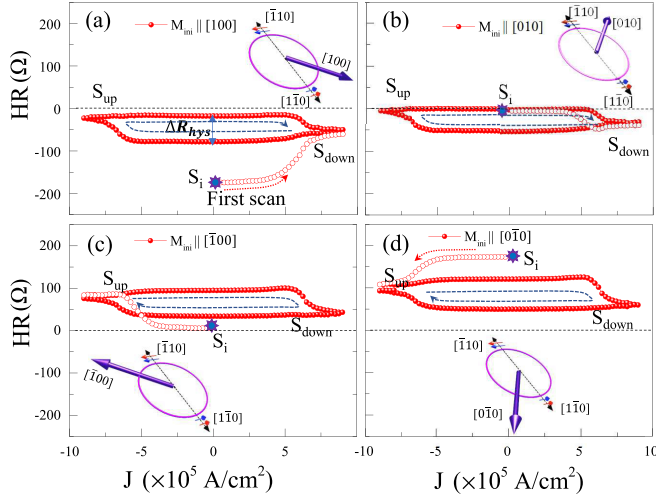


FIG. 4. (a)–(d) HR data observed by current scans for magnetization initialized along four different easy axes. The first scan for each initial orientation of magnetization is plotted with open symbols. The initial, down, and up states in the hysteresis are marked as S_i , S_{down} , and S_{up} , respectively. The difference between S_{down} and S_{up} at zero field is marked as ΔR_{hys} . The star symbol indicates the initial value of HR at state S_i . The dotted red arrow in (a) shows the direction of the first scan. The insets of each panel show initialized directions (thick violet arrow) and Dresselhaus (red arrow) and Rashba (blue arrow) SOFs corresponding to positive and negative currents (dotted black arrows). Switching chirality in the HR hysteresis loops is always clockwise (CW) regardless of the initial directions of magnetization, as indicated by dashed arrows inside each hysteresis loop.

magnetization into the film plane, reducing the $|\text{AHR}|$ while increasing $|\text{PHR}|$. This realizes the condition of $|\text{AHR}| < |\text{PHR}|$, resulting in small positive and negative HR values, respectively, at the B and C states shown in Fig. 3(a).

Successive current scans between $+9 \times 10^5 \text{ A/cm}^2$ ($I = +3.6 \text{ mA}$) and $-9 \times 10^5 \text{ A/cm}^2$ ($I = -3.6 \text{ mA}$) show a clear HR hysteresis loop with transitions between two stable HR states, indicating SOT-induced magnetization switching in the absence of an external magnetic field. Such field-free SOT switching loops show several interesting features. First, the change in the Hall resistance ΔR_{hys} between stable states is only about $\sim 70 \text{ } \Omega$, much smaller than the $\sim 400 \text{ } \Omega$ change observed in angular scans of HR shown in Fig. 3(a), clearly indicating that the switching of magnetization defining the hysteresis is partial, rather than involving the entire magnetization of the sample. Second, when the initialized magnetizations are in the $[100]$ and $[010]$ directions (i.e., in the first and second quadrants), the HR hysteresis appears only in the negative HR region [see Figs. 4(a) and 4(b)], while they appear always at the positive HR region when the magnetization is initialized in the $[\bar{1}00]$ and $[0\bar{1}0]$ directions (i.e., third and fourth quadrants), as seen in Figs. 4(c) and 4(d) indicating a vertical shift in the HR hysteresis loop. Third, the switching chirality of the HR hysteresis loops is always clockwise (CW), regardless of the directions in which magnetization is initialized, as shown by dotted curves inside of the loops in Fig. 4. Fourth, the two stable states in HR hysteresis consistently repeat over many back and forth current scans for all initial

directions of magnetization (see Supplemental Sec. 2 [35]) regardless of the first starting current scan direction (either positive or negative), assuring stability and reproducibility of the observed HR states.

The observed SOT magnetization switching can be described by the Landau-Lifshitz-Gilbert (LLG) equation, which includes contributions from both dampinglike torque (DLT) and fieldlike torque (FLT). However, it has been shown that the DLT, given by $\mathbf{M} \times (\boldsymbol{\sigma} \times \mathbf{M})$, where $\boldsymbol{\sigma}$ is the spin polarization of the carriers, plays a dominant role in current-induced magnetization switching in GaAs-based ferromagnetic semiconductors such as (Ga,Mn)(As) and (Ga,Mn)(As,P) films [11,40,41]. The direction of $\mathbf{M} \times (\boldsymbol{\sigma} \times \mathbf{M})$ is the same as the spin polarization $\boldsymbol{\sigma}$, which is perpendicular to the $[1\bar{1}0]$ current direction within the film plane [see Fig. 2(d)]. As obtained from analyzing the angular dependence of PHR (see Fig. 3(b) and Supplemental Sec. 1 [35]), our (Ga,Mn)(As,P) film exhibits strong fourfold magnetic anisotropy in the (001) crystal plane, with energy minima along the $\langle 100 \rangle$ directions. When the DLT has a component along one of the magnetic easy axes, it pushes the magnetization to transition to that easy axis. Then the magnetization transition occurs via a 90° rotation between the four easy magnetization directions ($[100]$, $[010]$, $[\bar{1}00]$, and $[0\bar{1}0]$). The detailed SOT transition process for the (Ga,Mn)(As,P) film with strong fourfold in-plane magnetic anisotropy is well described by Han *et al.*, in Ref. [26]. The transition of magnetization in FMS films is known to occur via domain nucleation and expansion [42,43]. In SOT magnetization switching of the FMS film, the same process occurs during the current scan. The degree of nucleation and expansion of new domains depends on the domain pinning energy of the sample, which is distributed over the film [44]. Such fluctuation in the magnetic properties of the film can lead to a partial SOT switching in the FMS film.

VI. CALCULATION OF MAGNETIC CONFIGURATIONS OF THE STABLE HR STATES

Magnetic configurations for the stable HR states observed in the vicinal sample during SOT switching can be obtained by analyzing the HR hysteresis using Eq. (6). As seen in Fig. 4, the starting HR values for magnetizations initialized at $[100]$, $[010]$, $[\bar{1}00]$, and $[0\bar{1}0]$ are, respectively, $\sim -175 \text{ } \Omega$, $\sim -5 \text{ } \Omega$, $\sim 5 \text{ } \Omega$, and $\sim 175 \text{ } \Omega$. Since for these initial points the total magnetization M_0 lies along the respective easy axes (i.e., at $\varphi_M = 45^\circ$, 135° , 225° , or 315°), the initial values of HR can be expressed using Eq. (6): Then, the observed HR values for the four initial magnetization directions can be related to the combined contribution of AHR and PHR as

$$\begin{aligned} \text{HR}_{[100]} &= -\frac{R_s}{t} M_0 \frac{\sqrt{2}}{2} \sin \alpha + \frac{k}{t} M_0^2 \left(1 - \frac{1}{2} \sin^2 \alpha \right) \\ &= -A + B \approx -175, \end{aligned} \quad (7a)$$

$$\begin{aligned} \text{HR}_{[010]} &= -\frac{R_s}{t} M_0 \frac{\sqrt{2}}{2} \sin \alpha - \frac{k}{t} M_0^2 \left(1 - \frac{1}{2} \sin^2 \alpha \right) \\ &= -A - B \approx -5, \end{aligned} \quad (7b)$$

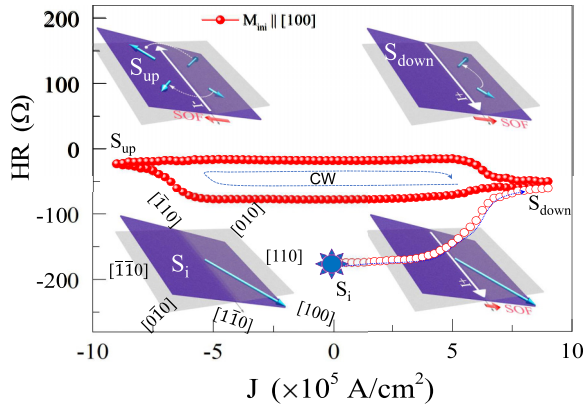


FIG. 5. SOT-induced HR hysteresis measured by scanning the current after magnetization is initialized along the $[100]$ direction. Insets show magnetization alignments at the initialized (S_i), the up (S_{up}), and the down state (S_{down}). The thick sky-blue arrows in the (001) crystal plane (violet plane) indicate directions of magnetization for S_i , S_{up} , and S_{down} states. The star symbol indicates the initial HR value of the scan. Open circles show HR values of the first current scan to $+9 \times 10^5$ A/cm 2 , and the blue curved arrow indicates the first scan direction. Long white arrow and thick red arrows in the insets show the current direction and corresponding SOF directions, respectively.

$$\begin{aligned} \text{HR}_{[1\bar{1}00]} &= \frac{R_s}{t} M_0 \frac{\sqrt{2}}{2} \sin \alpha + \frac{k}{t} M_0^2 \left(1 - \frac{1}{2} \sin^2 \alpha\right) \\ &= A + B \approx 5, \end{aligned} \quad (7c)$$

$$\begin{aligned} \text{HR}_{[0\bar{1}0]} &= \frac{R_s}{t} M_0 \frac{\sqrt{2}}{2} \sin \alpha - \frac{k}{t} M_0^2 \left(1 - \frac{1}{2} \sin^2 \alpha\right) \\ &= A - B \approx 175, \end{aligned} \quad (7d)$$

where terms A and B represent the AHR and PHR contributions, respectively. From Eq. (7) we obtain $A \approx 90$ Ω and $B \approx -85$ Ω . The fact that the values of A and B are close arises from the specific inclination of our sample, resulting in the near cancellation of AHR and PHR seen in quadrants 2 and 3 as seen in Fig. 3(a).

As an example, we consider the SOT current-scan hysteresis obtained for magnetization initialized in the $[100]$ in greater detail [data shown in Fig. 4(a), replotted in Fig. 5].

The initial, the down, and the up states of the hysteresis are marked S_i , S_{down} , and S_{up} , respectively. Note that after the first current scan to $+9 \times 10^5$ A/cm 2 the HR stabilizes at the S_{down} state at approximately -71 Ω (see data with open circles in Fig. 5). In the subsequent current scan, from $+9 \times 10^5$ A/cm 2 to -9×10^5 A/cm 2 , HR makes a transition to the S_{up} state (~ -15 Ω) as the negative current exceeds $\sim 6.25 \times 10^5$ A/cm 2 . In the return scan (i.e., -9×10^5 A/cm 2 to $+9 \times 10^5$ A/cm 2), HR switches back to the S_{down} state after the positive current reaches $\sim 6.25 \times 10^5$ A/cm 2 , completing the single hysteresis loop. Importantly, neither the S_{down} nor the S_{up} state reaches the maximum magnitude of $\sim |175|$ Ω (i.e., the value of HR at S_i) seen in Fig 5, indicating that only a fraction of the initial magnetization participates in the back and forth current scans that form the HR hysteresis.

As an example, we now consider the partial reorientation of magnetic domains as the current is swept from state S_i to form the stable state S_{down} (open symbols in Fig. 5). The positive current (i.e., current flowing in the $[1\bar{1}0]$ direction) induces SOFs along the $[110]$ direction, as shown by thick red arrows in the lower- and upper-right insets [see also Fig. 2(d)]. When the current value is low (below $\sim 5 \times 10^5$ A/cm 2), the SOF is too weak to produce magnetization switching (lower-right inset). As the SOF becomes stronger with further increase of the current (beyond $\sim 6.25 \times 10^5$ A/cm 2), the torque due to the spin polarization of the current along $[110]$ eventually become sufficiently strong to switch some of the magnetization from $[100]$ to $[010]$. Note that this occurs in the absence of an external magnetic field. Such field-free SOT switching process in a crystalline FMS film with fourfold in-plane anisotropy has already been reported by Han *et al.* [26], who demonstrated that the presence of a SOF component along in-plane easy axes causes current-induced field-free magnetization switching. Since, as noted earlier, we know that the SOT switching of magnetization observed in current sweeps is only partial, the stable state observed with positive current in Fig. 5 (i.e., state marked S_{down}) consists of magnetization both along the original $[100]$ direction and along $[010]$, as schematically shown in the upper-right inset in Fig. 5.

We will now estimate the volume fractions of magnetization along these two directions for the S_{down} state using Eq. (7). Since the film magnetization in this state consists of $[100]$ and $[010]$ components, and HR is approximately -71 Ω , we use Eq. (7) to write

$$\begin{aligned} \text{HR}(S_{down}) &= \left[-\frac{R_s}{t} M_{[100]} \frac{\sqrt{2}}{2} \sin \alpha + \frac{k}{t} M_{[100]}^2 \left(1 - \frac{1}{2} \sin^2 \alpha\right) - \frac{R_s}{t} M_{[010]} \frac{\sqrt{2}}{2} \sin \alpha - \frac{k}{t} M_{[010]}^2 \left(1 - \frac{1}{2} \sin^2 \alpha\right) \right] \\ &= -A(M_{[100]}) + B(M_{[100]}) - A(M_{[010]}) - B(M_{[010]}) \\ &= -A p_{[100]} + B p_{[100]}^2 - A p_{[010]} - B p_{[010]}^2 \approx -71 \Omega, \end{aligned} \quad (8)$$

where we replace M_0 in Eqs. (7a) and (7b) by magnetizations $M_{[100]}$ along $[100]$ and $M_{[010]}$ along $[010]$. Furthermore, since the original magnetization of the film is now divided between the $[100]$ and $[010]$ directions, we write $M_{[100]} = p_{[100]} M_0$, $M_{[010]} = p_{[010]} M_0$, with $p_{[100]} + p_{[010]} = 1$, where $p_{[100]}$ and $p_{[010]}$ are the respective volume fractions of magnetization

in the $[100]$ and $[010]$ directions, and M_0 is the total magnetization of the film. Since we already obtained the values $A \approx 90$ Ω and $B \approx -85$ Ω from the initialized states, as explained above, we can solve Eq. (8) for $p_{[100]}$ and $p_{[010]}$:

$$p_{[100]} \approx 0.39, \quad p_{[010]} \approx 0.61. \quad (9)$$

This indicates that in making the transition from S_i to S_{down} , about $\sim 61\%$ of magnetic domains magnetized along [100] switch to [010] magnetization, while $\sim 39\%$ remain as originally magnetized, as schematically indicated in the upper-right inset of Fig. 5.

The magnetizations in the [100] and [010] directions forming the S_{down} state remain stable as the positive current is reduced. When the current direction is reversed, SOF reverses to the $[\bar{1}\bar{1}0]$ direction (see thick red arrows in upper-left inset). As the value of the $[\bar{1}\bar{1}0]$ SOFs continues to increase, the torque on the [100] magnetization causes a partial switch of this magnetization to $[0\bar{1}0]$, and similarly a part of the [010] magnetization to switch to $[\bar{1}00]$, as shown by the dotted arrows in the upper-left inset. This establishes a new stable state S_{up} with a HR value of approximately -15Ω , made up of magnetizations along all four easy axes. The volume fractions of magnetization for this new state can be determined from

$$\begin{aligned} \text{HR}(S_{\text{up}}) = & \left[-Ap_{[100]} + Bp_{[100]}^2 - Ap_{[010]} - Bp_{[010]}^2 \right. \\ & \left. + Ap_{[\bar{1}00]} + Bp_{[\bar{1}00]}^2 + Ap_{[0\bar{1}0]} - Bp_{[0\bar{1}0]}^2 \right] \\ & \approx -15 \Omega, \end{aligned} \quad (10)$$

where we use the same procedure as in Eq. (8); i.e., we replace M_0 in Eq. (7) by $M_{[100]} = p_{[100]}M_0$, $M_{[010]} = p_{[010]}M_0$, $M_{[\bar{1}00]} = p_{[\bar{1}00]}M_0$, and $M_{[0\bar{1}0]} = p_{[0\bar{1}0]}M_0$, $p_{[100]}$ being the volume fractions of magnetization along the corresponding $\langle 100 \rangle$ directions. Furthermore, using Eq. (9), we have

$$p_{[100]} + p_{[0\bar{1}0]} \approx 0.39, \quad p_{[010]} + p_{[\bar{1}00]} \approx 0.61. \quad (11)$$

By using the values of $A = 90 \Omega$ and $B = -85 \Omega$, and Eq. (11), we can now solve Eq. (10) for the values of p along the four easy axes. The solution is straightforward, but somewhat cumbersome, and we defer its details to Supplemental Sec. 3 [35].

Here we will estimate the volume fractions applying a convenient shortcut. The reader will notice that the contribution of magnetizations in the second and third quadrants is almost negligible compared to those in the first and fourth quadrants, as seen in Fig. 3(a), and values are shown in Eq. (7). Considering only the transition from the first to the fourth quadrant, we can write, in analogy with Eq. (8),

$$\begin{aligned} \text{HR}(S_{\text{up}}) = & -A p_{[100]} + Bp_{[100]}^2 + A p_{[0\bar{1}0]} - Bp_{[0\bar{1}0]}^2 \\ & \approx -15 \Omega. \end{aligned} \quad (12)$$

Using $p_{[100]} + p_{[0\bar{1}0]} = 0.39$ from Eq. (11), we find that magnetization fractions distributed between [100] and $[0\bar{1}0]$ orientations are $p_{[100]} \approx 0.25$ and $p_{[0\bar{1}0]} \approx 0.14$. It is gratifying that the full calculation carried out in Supplemental Sec. 3 [35] gives values $p_{[100]} \approx 0.24$ and $p_{[0\bar{1}0]} \approx 0.15$, supporting the assumption made in this ‘‘shortcut’’ that the transition from [100] \rightarrow $[0\bar{1}0]$ (first \rightarrow fourth quadrant) represents the main contribution to the SOT hysteresis, so that as a good approximation the contribution from transition $[010] \rightarrow [\bar{1}00]$ (second \rightarrow third quadrant) can be ignored in the process of forming the hysteresis.

When the current direction is again changed back to positive, the system returns to the S_{down} state, indicating that the magnetizations at the $[\bar{1}00]$ and $[0\bar{1}0]$ axes return,

respectively, to the [010] and the [100] directions of that state. Thus magnetization transitions $[\bar{1}00] \leftrightarrow [010]$ and $[0\bar{1}0] \leftrightarrow [100]$ occur back and forth during the current scan between $+9 \times 10^5 \text{ A/cm}^2$ and $-9 \times 10^5 \text{ A/cm}^2$, forming the hysteresis seen in Fig. 5. The reproducibility of this hysteresis, as well as being analogous with hysteresis observed with magnetization initialized along the other three easy axes, is confirmed by many repeated current scans, as shown in Supplemental Fig. 2 [35].

VII. DISCUSSION

Current direction. Our choice of current direction, $(\bar{1}\bar{1}0)$ or $(\bar{1}10)$, is not arbitrary. As seen in Fig. 2(d), the SOFs due to both the Rashba and Dresselhaus effects produced by this current orientation add constructively, resulting in the strongest SOF torque, making this choice of current orientation optimal for observing field-free SOT switching of magnetization. Future experiments with currents in other crystallographic directions may be useful in resolving quantitatively the difference between the effects of Rashba and Dresselhaus interactions in the SOT process.

Chirality of HR hysteresis. The observed chirality of the HR hysteresis is unique to vicinal films, and can be ascribed to the roles played by AHR and PHR as a result of the inclination of the film and the crystal (001) planes. This can be easily seen by recognizing their respective contributions in the formation of hysteresis. From Fig. 3(a) it is clear that the contribution of magnetization in the second and third quadrants to the hysteresis is nearly negligible, so that the sense of the hysteresis is determined by the back and forth switching of magnetization between the first quadrant (where the sum of AHR and PHR makes HR strongly negative) and the fourth quadrant (where these two contributions make HR strongly positive). This chirality is the property of the inclination of the film relative to the (001) crystal plane, and does not depend on either the direction of the initialized magnetization or on the starting direction of the current scan. Specifically, the form of chirality arises from the presence of AHR that originates from the tilt of vicinal films, distinguishing them from FMS films grown on (001) planes, in which it does not exist [26]. In this context it may be interesting to carry out similar investigations on vicinal films tilted in different directions.

Partial switching of magnetization. As seen in Figs. 4 and 5, the difference ΔR_{hys} between S_{up} and S_{down} , the upper and lower states that define the hysteresis, is only about $\sim 70 \Omega$, much smaller than the value of $\sim 175 \Omega$ observed at S_i , when total magnetization of the film determines HR. Thus we must conclude that only a fraction (about 15%–20%) of magnetization switches back and forth as the current is scanned. Such partial SOT switching has been observed already in FMS film grown on a normal (001) substrate, and the switching process is illustrated in detail in Fig. 3 of Ref. [26]. It is tempting to ascribe this to differences in magnetic domain pinning, so that SOF is only sufficient to turn some domains, while others remain fixed. Unfortunately at present we do not have sufficient quantitative understanding of domain pinning in (Ga,Mn)(As,P), so that this important issue must await further studies.

Vertical shift of HR hysteresis. The vertical shift of the HR hysteresis loop toward the negative HR region for the [100]

and [010] direction initializations (first and second quadrants) and toward positive HR region in the $[\bar{1}00]$ and $[0\bar{1}0]$ direction (third and fourth quadrants) initializations are due to partial magnetization switching between the easy axes in the (001) plane by SOT as mentioned above. For magnetization initialized in either the [100] or [010] direction (first or second quadrants), a part of the magnetization remains in the first quadrant during the SOT switching process. This magnetization in the first quadrant contributes a negative value of HR (i.e., $-|\text{PHR}|$ and $-|\text{AHR}|$), which provides a background signal, shifting the entire SOT switching hysteresis to the negative HR region [see Figs. 4(a) and 4(b)]. However, when the magnetization is initialized in the $[\bar{1}00]$ or $[0\bar{1}0]$ direction (third or fourth quadrants), a part of the magnetization remains in the fourth quadrant during the SOT switching process. This magnetization in the fourth quadrant contributes a positive value of HR (i.e., $+|\text{PHR}|$ and $+|\text{AHR}|$), which provides a background signal, shifting the entire SOT switching hysteresis to the positive HR region [see Figs. 4(c) and 4(d)].

The above described SOT magnetization switching behaviors observed from our (Ga,Mn)(As,P) film grown on vicinal surface are somewhat different from that observed from a FePt system [45], in which field-free SOT switching was achieved due to the tilted magnetic anisotropy of the film. In a FMS system field-free SOT was achieved due to the presence of a spin polarization component along the magnetic easy axes. Specifically, carrier spin polarization in our (Ga,Mn)(As,P) film is achieved via the Dresselhaus and Rashba effects, resulting in diverse spin polarization directions (i.e., perpendicular, parallel, or antiparallel relative to the current direction), as shown in Fig. 2(d). Such diverse configurations between spin polarization and current direction cannot be realized in metal-based ferromagnetic systems, where carrier spin polarization is achieved via the spin Hall effect and is always perpendicular to the current direction. Some interesting SOT switching phenomena arising from collinear configurations between spin polarization and current direction have been observed in FMS films in previous works [14,46]. While SOT phenomena arising from such diverse configurations of spin polarization have not been investigated in the current study, further interesting SOT phenomena are expected from FMS films grown on vicinal surfaces. This underscores the importance of our present investigation as a step for SOT research based on FMS films grown on vicinal surfaces.

VIII. SUMMARY

In summary, we investigated the field-free magnetization SOT switching in a single layer of crystalline (Ga,Mn)(As,P) film grown on a vicinal surface. HR values observed for the four easy magnetization directions arising from the four-fold magnetic anisotropy in the (001) crystal plane are well resolved due to the tilted angle between the (001) crystal plane and the sample plane, which causes the presence of both in-plane and out of plane components of magnetization

with respect to the sample plane. Field-free SOT magnetization switching was achieved by sweeping the current for the four magnetization directions initialized along the four easy axes (i.e., $\langle 100 \rangle$ directions) in the (001) crystal plane. The resulting HR hysteresis is highly reproducible over many current sweeps, indicating the stability of the S_{down} and S_{up} states. Magnetic configurations of these stable states were determined by solving the HR equation for the vicinal sample that includes both AHR and PHR contributions. Importantly, the results of these experiments indicate that the switching of magnetization in the observed transitions is partial switching between easy axes, suggesting that the degree of pinning may be different for different domains. The mechanism of such pinning is not understood at present. The observed HR hysteresis loops are formed by two back and forth magnetization switching processes, $[010] \leftrightarrow [\bar{1}00]$ and $[100] \leftrightarrow [0\bar{1}0]$. However, even though two back and forth magnetization switchings are involved, in the case of the specific sample tilt of our film (about the $[\bar{1}\bar{1}0]$ crystal axis), the $[100] \leftrightarrow [0\bar{1}0]$ transition (i.e., when magnetization switches between the first and the fourth quadrants) dominates the HR hysteresis formation, determining its chirality in current scan HR hysteresis loops. Importantly, this study demonstrates that the magnetization in a (Ga,Mn)(As,P) crystal film grown on a vicinal surface can be manipulated by SOT in the absence of an external field, thus providing valuable insights for developing multilevel field-free memory devices. Even though we have focused on the magnetization switching behavior using as-grown (Ga,Mn)(As,P) film at low temperature, where magnetic easy axes are well defined along the $\langle 100 \rangle$ crystal direction, the SOT switching experiment on the (Ga,Mn)(As,P) films grown on a vicinal surface is still in its early stages. The magnetic properties and crystallinity of the (Ga,Mn)(As,P) film may change with thermal annealing, which can affect the SOT switching process. The effect of thermal annealing on SOT switching of the FMS film grown on a vicinal surface is certainly an interesting subject that needs to be investigated in the future.

The data supporting the findings of this study are available from the corresponding author on request.

ACKNOWLEDGMENTS

This research was supported by the Basic Science Research Program through the National Research Foundation of Korea (NRF) (Grant No. 2021R1A2C1003338); by the National Research Foundation of Korea (NRF) grant funded by the Korea government (MSIT) (Grant No. 2022M3F3A2A03014536); by the NRF under the BK21 FOUR program at Korea University, Initiative for Science Frontiers on Upcoming Challenges; by Korea University Grant; and by National Science Foundation Grant No. DMR 1905277.

The authors have no conflicts of interest to disclose.

[1] X. Han, X. Wang, C. Wan, G. Yu, and X. Lv, Spin-orbit torques: Materials, physics, and devices, *Appl. Phys. Lett.* **118**, 120502 (2021).

[2] Q. Shao, P. Li, L. Liu, H. Yang, S. Fukami, A. Razavi, H. Wu, K. Wang, F. Freimuth, Y. Mokrousov *et al.*, Roadmap of spin-orbit torques, *IEEE Trans. Magn.* **57**, 1 (2021).

- [3] C. Song, R. Zhang, L. Liao, Y. Zhou, X. Zhou, R. Chen, Y. You, X. Chen, and F. Pan, Spin-orbit torques: Materials, mechanisms, performances, and potential applications, *Prog. Mater. Sci.* **118**, 100761 (2021).
- [4] F. Oboril, R. Bishnoi, M. Ebrahimi, and M. B. Tahoori, Evaluation of hybrid memory technologies using SOT-MRAM for on-chip cache hierarchy, *IEEE Trans. Comput.-Aided Des. Integr. Circuits Syst.* **34**, 367 (2015).
- [5] H. Lin, X. Luo, L. Liu, D. Wang, X. Zhao, Z. Wang, X. Xue, F. Zhang, and G. Xing, All-electrical control of compact SOT-MRAM: Toward highly efficient and reliable non-volatile in-memory computing, *Micromachines* **13**, 319 (2022).
- [6] V. Lopez-Dominguez, Y. Shao, and P. Khalili Amiri, Perspectives on field-free spin-orbit torque devices for memory and computing applications, *J. Appl. Phys.* **133**, 040902 (2023).
- [7] Y. Song, Z. Dai, L. Liu, J. Wu, T. Li, X. Zhao, W. Liu, and Z. Zhang, Field-free spin-orbit torque switching of perpendicular magnetization by making full use of spin Hall effect, *Adv. Electron. Mater.* **9**, 2200987 (2023).
- [8] M. H. Lee, G. Go, Y. J. Kim, I. H. Cha, G. W. Kim, T. Kim, K.-J. Lee, and Y. K. Kim, Spin-orbit torques in normal metal/Nb/ferromagnet heterostructures, *Sci. Rep.* **11**, 21081 (2021).
- [9] Y. Li, Y. F. Cao, G. N. Wei, Y. Li, Y. Ji, K. Y. Wang, K. W. Edmonds, R. P. Campion, A. W. Rushforth, C. T. Foxon *et al.*, Anisotropic current-controlled magnetization reversal in the ferromagnetic semiconductor (Ga,Mn)As, *Appl. Phys. Lett.* **103**, 022401 (2013).
- [10] S. Lee, S. Choi, S. Bac, K. J. Lee, J. Chang, S. Choi, P. Chongthanaphisut, S. Lee, X. Liu, M. Dobrowolska *et al.*, Determination of current-induced spin-orbit effective magnetic field in GaMnAs ferromagnetic semiconductor, *Appl. Phys. Lett.* **111**, 252401 (2017).
- [11] M. Jiang, H. Asahara, S. Sato, S. Ohya, and M. Tanaka, Suppression of the field-like torque for efficient magnetization switching in a spin-orbit ferromagnet, *Nat. Electron.* **3**, 751 (2020).
- [12] S. Park, K. J. Lee, S. Lee, X. Liu, M. Dobrowolska, and J. K. Furdyna, Spin-orbit torque switching in a single (Ga,Mn)(As,P) layer with perpendicular magnetic anisotropy, *APL Mater.* **9**, 101102 (2021).
- [13] K. Han, K. J. Lee, S. Lee, X. Liu, M. Dobrowolska, and J. K. Furdyna, Effect of spin-orbit field on magnetization reversal in GaMnAs single layers with 4-fold in-plane magnetic anisotropy, *AIP Adv.* **13**, 025229 (2023).
- [14] K. Han, K. J. Lee, S. Lee, X. Liu, M. Dobrowolska, and J. K. Furdyna, Investigation of orthogonal spin-orbit fields in crystalline ferromagnetic films with four-fold in-plane magnetic anisotropy, *APL Mater.* **11**, 051114 (2023).
- [15] H. X. Tang, R. K. Kawakami, D. D. Awschalom, and M. L. Roukes, Giant planar Hall effect in epitaxial (Ga,Mn)As devices, *Phys. Rev. Lett.* **90**, 107201 (2003).
- [16] K. J. Lee, K. Han, S. Lee, X. Liu, M. Dobrowolska, and J. K. Furdyna, Multilevel states driven by spin-orbit torque in a P-composition graded (Ga,Mn)(As,P) film, *AIP Adv.* **13**, 025122 (2023).
- [17] Y. Sheng, Y. C. Li, X. Q. Ma, and K. Y. Wang, Current-induced four-state magnetization switching by spin-orbit torques in perpendicular ferromagnetic trilayers, *Appl. Phys. Lett.* **113**, 112406 (2018).
- [18] J. Zhou, T. Zhao, X. Shu, L. Liu, W. Lin, S. Chen, S. Shi, X. Yan, X. Liu, and J. Chen, Spin-orbit torque-induced domain nucleation for neuromorphic computing, *Adv. Mater.* **33**, 2103672 (2021).
- [19] R. K. Kawakami, E. J. Escorcía-Aparicio, and Z. Q. Qiu, Symmetry-induced magnetic anisotropy in Fe films grown on stepped Ag(001), *Phys. Rev. Lett.* **77**, 2570 (1996).
- [20] S. Ma, A. Tan, J. X. Deng, J. Li, Z. D. Zhang, C. Hwang, and Z. Q. Qiu, Tailoring the magnetic anisotropy of Py/Ni bilayer films using well aligned atomic steps on Cu(001), *Sci. Rep.* **5**, 11055 (2015).
- [21] S. S. Dhesi, H. A. Dürr, and G. van der Laan, Canted spin structures in Ni films on stepped Cu(001), *Phys. Rev. B* **59**, 8408 (1999).
- [22] W. L. Lim, X. Liu, K. Dziatkowski, Z. Ge, S. Shen, J. K. Furdyna, and M. Dobrowolska, Effect of magnetic anisotropy on the transverse planar Hall resistance of $\text{Ga}_{1-x}\text{Mn}_x\text{As}$ films grown on vicinal GaAs substrates, *Phys. Rev. B* **74**, 045303 (2006).
- [23] W. L. Lim, X. Liu, K. Dziatkowski, Z. Ge, S. Shen, J. K. Furdyna, and M. Dobrowolska, Investigation of magnetocrystalline anisotropy by planar Hall effect in GaMnAs epilayers grown on vicinal GaAs substrates, *J. Appl. Phys.* **99**, 08D505 (2006).
- [24] X. Liu, J. K. Furdyna, M. Dobrowolska, W. L. Lim, C. Xie, and Y. J. Cho, Unique properties of magnetotransport in GaMnAs films grown on vicinal and high-index planes, *J. Phys.: Condens. Matter* **19**, 165205 (2007).
- [25] Y. Tao, C. Sun, W. Li, L. Yang, F. Jin, Y. Hui, H. Li, X. Wang, and K. Dong, Field-free spin-orbit torque switching in $L1\text{-FePt}$ single layer with tilted anisotropy, *Appl. Phys. Lett.* **120**, 102405 (2022).
- [26] K. Han, K. J. Lee, S. Lee, X. Liu, M. Dobrowolska, and J. K. Furdyna, Field-free spin-orbit-torque switching of a single ferromagnetic layer with fourfold in-plane magnetic anisotropy, *APL Mater.* **11**, 081114 (2023).
- [27] C. H. Wan, M. E. Stebliy, X. Wang, G. Q. Yu, X. F. Han, A. G. Kolesnikov, M. A. Bazrov, M. E. Letushev, A. V. Ognev, and A. S. Samardak, Gradual magnetization switching via domain nucleation driven by spin-orbit torque, *Appl. Phys. Lett.* **118**, 032407 (2021).
- [28] S. Kim, H. Lee, T. Yoo, S. Lee, S. Lee, X. Liu, and J. K. Furdyna, Mapping of magnetic anisotropy in strained ferromagnetic semiconductor GaMnAs films, *J. Appl. Phys.* **107**, 103911 (2010).
- [29] S.-K. Bac, H. Lee, S. Lee, S. Choi, S. Lee, X. Liu, M. Dobrowolska, and J. K. Furdyna, Effects on magnetic properties of GaMnAs induced by proximity of topological insulator Bi_2Se_3 , *J. Electron. Mater.* **47**, 4308 (2018).
- [30] G. B. Arfken, H.-J. Weber, and F. E. Harris, *Mathematical Methods for Physicists: A Comprehensive Guide*, 7th ed. (Academic Press, Waltham, MA, 2013).
- [31] Y. Y. Zhou, X. Liu, J. K. Furdyna, M. A. Scarpulla, and O. D. Dubon, Ferromagnetic resonance study of $\text{Ga}_{1-x}\text{Mn}_x\text{As}$ fabricated on (311) GaAs wafers by Mn ion implantation and pulsed-laser melting, *J. Supercond. Novel Magn.* **23**, 87 (2010).
- [32] S. Dong, Y.-L. Wang, S.-K. Bac, X. Liu, V. Vlasko-Vlasov, W.-K. Kwok, S. Rouvimov, S. Lee, M. Dobrowolska, and J. K. Furdyna, Programmable bias field observed in graded

- ferromagnetic semiconductor films with broken symmetry, *Phys. Rev. Mater.* **3**, 074407 (2019).
- [33] R. F. Need, S.-K. Bac, X. Liu, S. Lee, B. J. Kirby, M. Dobrowolska, J. Kossut, and J. K. Furdyna, Magnetic properties and electronic origin of the interface between dilute magnetic semiconductors with orthogonal magnetic anisotropy, *Phys. Rev. Mater.* **4**, 054410 (2020).
- [34] Sh. U. Yuldashev, H. Im, V. Sh. Yalishev, C. S. Park, T. W. Kang, S. Lee, Y. Sasaki, X. Liu, and J. K. Furdyna, Effect of additional nonmagnetic acceptor doping on the resistivity peak and the curie temperature of $\text{Ga}_{1-x}\text{Mn}_x\text{As}$ epitaxial layers, *Appl. Phys. Lett.* **82**, 1206 (2003).
- [35] See Supplemental Material at <http://link.aps.org/supplemental/10.1103/PhysRevB.110.054422> for additional information about the angle scan measurement data at different in plane magnetic field strengths, repeated SOT current scan hysteresis loop measurements at four $\langle 100 \rangle$ easy axes initialized directions to check the stability and reproducibility of HR states, and detailed calculations of the volume fraction of magnetization for the stable HR states in the four $\langle 100 \rangle$ easy axes initialized directions.
- [36] S. Lee, T. Yoo, S.-K. Bac, S. Choi, H. Lee, S. Lee, X. Liu, M. Dobrowolska, and J. K. Furdyna, Field-free manipulation of magnetization alignments in a Fe/GaAs/GaMnAs multilayer by spin-orbit-induced magnetic fields, *Sci. Rep.* **7**, 10162 (2017).
- [37] D. Y. Shin, S. J. Chung, S. Lee, X. Liu, and J. K. Furdyna, Temperature dependence of magnetic anisotropy in ferromagnetic (Ga,Mn)As films: Investigation by the planar Hall effect, *Phys. Rev. B* **76**, 035327 (2007).
- [38] G. Dresselhaus, Spin-orbit coupling effects in zinc blende structures, *Phys. Rev.* **100**, 580 (1955).
- [39] Y. A. Bychkov and E. I. Rashba, Oscillatory effects and the magnetic susceptibility of carriers in inversion layers, *J. Phys. C: Solid State Phys.* **17**, 6039 (1984).
- [40] M. Jiang, H. Asahara, S. Sato, T. Kanaki, H. Yamasaki, S. Ohya, and M. Tanaka, Efficient full spin-orbit torque switching in a single layer of a perpendicularly magnetized single-crystalline ferromagnet, *Nat. Commun.* **10**, 2590 (2019).
- [41] A. K. Jana and S. Lee, Investigation of spin-orbit torque switching mechanism in crystalline ferromagnetic semiconductor, *Appl. Phys. Lett.* **123**, 152401 (2023).
- [42] U. Welp, V. K. Vlasko-Vlasov, X. Liu, J. K. Furdyna, and T. Wojtowicz, Magnetic domain structure and magnetic anisotropy in $\text{Ga}_{1-x}\text{Mn}_x\text{As}$, *Phys. Rev. Lett.* **90**, 167206 (2003).
- [43] D. Y. Shin, S. J. Chung, S. Lee, X. Liu, and J. K. Furdyna, Stable multidomain structures formed in the process of magnetization reversal in GaMnAs ferromagnetic semiconductor thin films, *Phys. Rev. Lett.* **98**, 047201 (2007).
- [44] J. Kim, H. Lee, T. Yoo, S. Lee, X. Liu, and J. K. Furdyna, Effect of pinning-field distribution on the process of magnetization reversal in $\text{Ga}_{1-x}\text{Mn}_x\text{As}$ films, *Phys. Rev. B* **84**, 184407 (2011).
- [45] Y. Luo, Y. Zhuang, Z. Feng, H. Fan, B. Wu, M. Jin, Z. Shao, H. Li, R. Bai, Y. Wu *et al.*, Field-free switching through bulk spin-orbit torque in $L1_0$ -FePt films deposited on vicinal substrates, *Front. Phys.* **17**, 53511 (2022).
- [46] S. Park, K. J. Lee, K. Han, S. Lee, X. Liu, M. Dobrowolska, and J. K. Furdyna, Spin orbit torque switching of magnetization in the presence of two different orthogonal spin-orbit magnetic fields, *Appl. Phys. Lett.* **121**, 112403 (2022).